



Fabrication, Microstructure and Mechanical Properties of in situ GNPs Reinforced Magnesium Matrix Composites

Peitang Zhao¹ · Xuejian Li² · Hailong Shi² · Xiaoshi Hu² · Chunlei Zhang² · Chao Xu² · Xiaojun Wang²

Received: 23 November 2022 / Revised: 8 January 2023 / Accepted: 26 January 2023 / Published online: 15 April 2023
© The Chinese Society for Metals (CSM) and Springer-Verlag GmbH Germany, part of Springer Nature 2023

Abstract

Graphene reinforced magnesium matrix composites have wide applications in automotive, electronics, aerospace and military fields due to the fascinating mechanical properties. However, it is difficult to realize the high strength and ductility simultaneously. In this work, the in situ liquid-state method was utilized to prepare GNPs/Mg₆Zn composites via CO₂/Mg chemical reaction. Tensile strength of the GNPs/Mg₆Zn composites was improved with increasing content of the GNPs. Meantime, the composites also exhibit a notable plastic deformation stage, and especially the ductility of 0.12 GNPs/Mg₆Zn composites reaches 27.6%. Therefore, this novel preparation method has great potential application for fabricating Mg matrix composites with high strength and high ductility.

Keywords Magnesium matrix composite · In situ composite · Microstructure · Mechanical properties

1 Introduction

Magnesium (Mg) matrix composites is the lightest structural material, which can greatly improve system performance and energy efficiency in automotive, electronics, aerospace and military fields [1–3]. In traditional Mg matrix composites, the use of micron-sized reinforcements (such as SiC, TiC and TiB) with high volume fraction (≥ 10 vol.%) has improved the strength significantly [4–6]. Unfortunately, it has also led to a sharp decline in ductility and the occurrence of the overall brittleness, which has greatly limited the application of Mg matrix composites. In comparison, nanosized reinforcement has shown excellent strengthening efficiency by virtue of their unique size effect. The

as-fabricated composites offer the opportunity to obtain high strength while maintaining good ductility simultaneously.

Graphene is a two-dimensional material with only one atomic layer thickness. The intrinsic fracture strength and elastic modulus of graphene are 130 GPa and 1 TPa, respectively [7–11]. Thus, graphene or graphene nanoplates (GNPs) are considered as an ideal reinforcement for Mg matrix due to the excellent mechanical properties and good chemical compatibility. However, GNPs have huge specific surface area and strong chemical activity, which makes it extremely difficult for GNPs to disperse in the Mg matrix. Thus, the preparation technology has become a main issue in the research of GNPs reinforced Mg matrix composites. At present, powder metallurgy is a widely used preparation method of metal matrix composites, especially in copper and aluminum matrix [12, 13]. Chen et al. [14] successfully fabricated GNPs/Cu composite with 0.6 vol.% addition of GNPs via powder metallurgy. The yield strength was improved evidently about 118%. Liu et al. [15] reported that 0.7 wt% GNPs reinforced Al matrix composites also showed a high yield strength of 140 MPa together with a tensile strength of 213 MPa. Unfortunately, it is a major challenge to prepare Mg matrix composite by powder metallurgy due to the flammability, explosion and oxidation of Mg powder [16, 17]. In contrast, GNPs does not react with Mg and can coexist with Mg melt for a long time at elevated

Available online at <http://link.springer.com/journal/40195>.

✉ Xuejian Li
lixuejian@hit.edu.cn

✉ Hailong Shi
hailongshi@hit.edu.cn

¹ The 38th Research Institute of China Electronics Technology Group Corporation, Hefei 230088, China

² National Key Laboratory of Precision Hot Processing of Metal, Harbin Institute of Technology, Harbin 150001, China

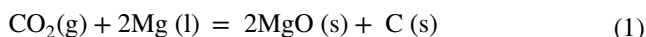
temperatures. Thus, liquid metallurgy process may be the better method for preparing Mg matrix composites. In recent years, Xiang et al. [18] developed a liquid-state metallurgy method (pre-dispersion, mechanical stirring and ultrasonic vibration) to prepare GNPs/Mg6Zn composites. However, the ductility of the composite is very poor owing to the obvious agglomeration of GNPs. On this foundation, Wang et al. further improves its dispersion via in situ reactive wetting process, which provides a novel idea into interfacial modification of advanced Mg matrix composites with high strength and ductility. Specifically, the interface product MgO is generated by in situ chemical reaction of ZnO coating on GNPs surface with molten Mg, which effectively improves the wettability in GNPs/Mg interfacial area and achieves excellent dispersion. Thus, the as-prepared Mg matrix composite realizes high strength and ductility [19]. Inspired by this, our previous work has developed an in situ liquid-state method by converting CO₂ to GNPs. GNPs can be directly formed in Mg matrix by chemical reaction of carbon dioxide (CO₂) gas and liquid Mg melt, and the surface of GNPs is also modified by MgO nanoparticles. This in situ liquid-state method has great potential to product GNPs reinforced Mg matrix composite with high strength and ductility [20, 21].

In this study, the in situ liquid-state method was selected to produce GNPs/Mg6Zn composites via CO₂/Mg chemical reaction. The interfacial structure and distribution of GNPs were studied systematically in Mg matrix. The results show that low content GNP in the composites also can adjust the microstructure and dramatically improve the overall strength and ductility compared with the Mg matrix. This study proves the feasibility of preparing Mg matrix composites with high strength and high ductility by in situ liquid-state method, which is called upon to promote its engineering application.

2 Experimental

2.1 Material preparation

Figure 1 shows the fabrication method of the GNPs/Mg6Zn composites. Three main parts were displayed including the in situ reaction, die casting and hot extrusion in a typical fabrication process. First, pure Mg was heated at 700 °C, and then the pure Zn was introduced to the crucible after the Mg melted. The addition of Zn element can reduce the melting point of the Mg alloy to avoid oxidation. In addition, Zn reacts with neither CO₂ nor graphene. Afterward, the temperature of mixture was reduced to 680 °C, and the CO₂ was added to Mg alloy melt with specific flow rate (900 ml/min) under the action of the aerator. It is worth noting that the entire liquid process was carried out under the protective gas of SF₆ and CO₂ (1:40). Thus, MgO modified GNPs can be formed via the in situ reaction of molten Mg and CO₂, which could be displayed by the following reaction:



With the introduction of CO₂, high-quality GNPs was generated continuously in Mg alloy melt. In this work, the composites with different contents of GNPs (0.12 and 0.28 vol.%) were prepared by controlling the supply of CO₂ bubbles. The as-prepared composites were named *x*GNPs/Mg6Zn composites (*x*=0.12 and 0.28 vol.%). More details were outlined in literature [20, 21]. After then, the slurry was solidified at a pressure of 100 MPa to eliminate air holes in ingots. The extrusion was carried out at 300 °C, the extrusion speed was 0.1 mm s⁻¹ and extrusion ratio was 12:1. At the same time, the Mg6Zn matrix was also prepared under the same parameters as the control.

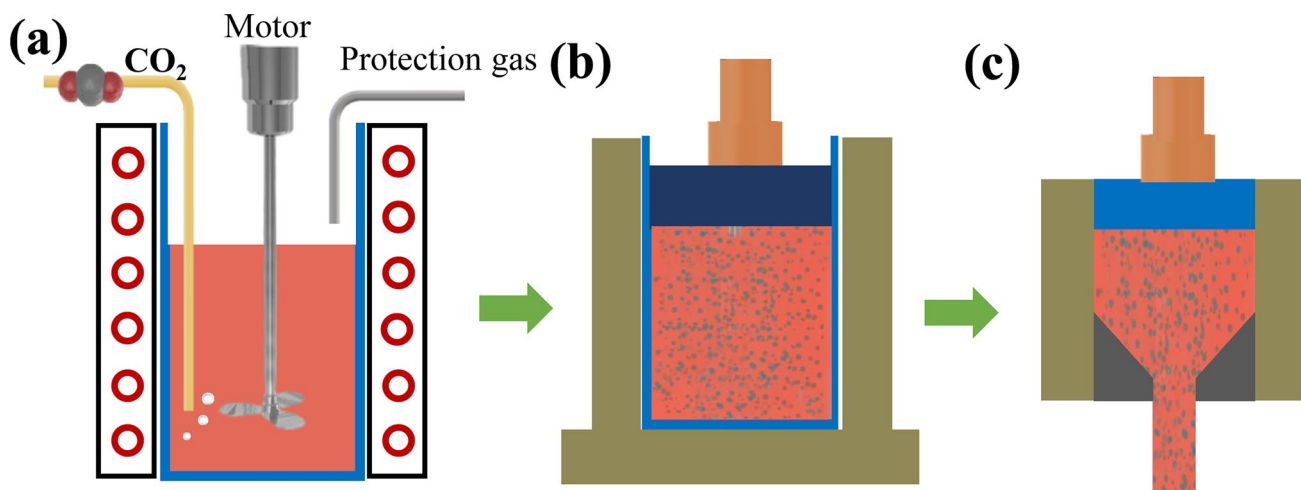


Fig. 1 Fabrication of GNPs/Mg6Zn composites: **a** in situ process; **b** die-casting; **c** hot extrusion

2.2 Material Characterization

The content of GNPs in the composite can be determined by the following process. First, the composite was immersed in H_2SO_4 solution to remove Mg6Zn matrix and MgO. Then, GNPs suspension liquid was washed and filtered with deionized water. Finally, GNPs powder was obtained after dried in a vacuum drying chamber. Thus, the content of GNPs can be determined by weighing GNPs powder and GNPs/Mg6Zn composite.

The X-ray diffraction (XRD) was conducted on with Cu $K\alpha$ radiation of 0.154 nm using X-ray diffractometer. Raman spectra were obtained by using a Raman Station to analyze the structural characteristics with a wavelength of 532 nm (B&WTEK, BWS435-532SY). The grain size of the Mg6Zn alloy and composites was analyzed using optical microscopy (OM). The dispersion and the microstructure in the GNPs/Mg6Zn composite were studied by scanning electron microscopy (SEM, SUPRA 55 SAPHIRE). Transmission electron microscopy (TEM, Talos F200x) was used to characterize the distribution of GNPs and the interfaces between the GNPs and the Mg matrix. Mechanical properties of samples were tested by using an electronic universal testing machine (Instron 5569) with the 1.0 mm min^{-1} tensile speed. The sizes of the

specimens were width of 5 mm, thickness of 2 mm and gauge length of 15 mm.

3 Results and Discussion

3.1 In situ Growth of GNPs

Figure 2a displays XRD result of the GNPs powder obtained via immersing the bulk samples in H_2SO_4 solution. Three characteristic diffraction peaks (002), (100) and (101) of GNPs appear at about 26.2° , 42.4° and 45.3° , respectively. One strong characteristic peak corresponding to the (002) crystalline plane of graphene indicates that as-fabricated GNPs possesses excellent crystallinity [22–24]. Raman results of the obtained powder also show a D band at 1347 cm^{-1} , a G band at 1578 cm^{-1} and a 2D band at 2687 cm^{-1} evidently in Fig. 2b. The positions of peak are in good agreement with typical graphene. The existence of the 2D band illustrates that the crystal structure has transformed from an amorphous state to graphitized state, and the blue shift of 2D also confirms that GNPs has fewer layers [25, 26]. In addition, the intensity ratio of D peak and G peak (I_D/I_G) is 0.56, which indicates that GNPs is under a low defect density. Furthermore, SEM and TEM images were

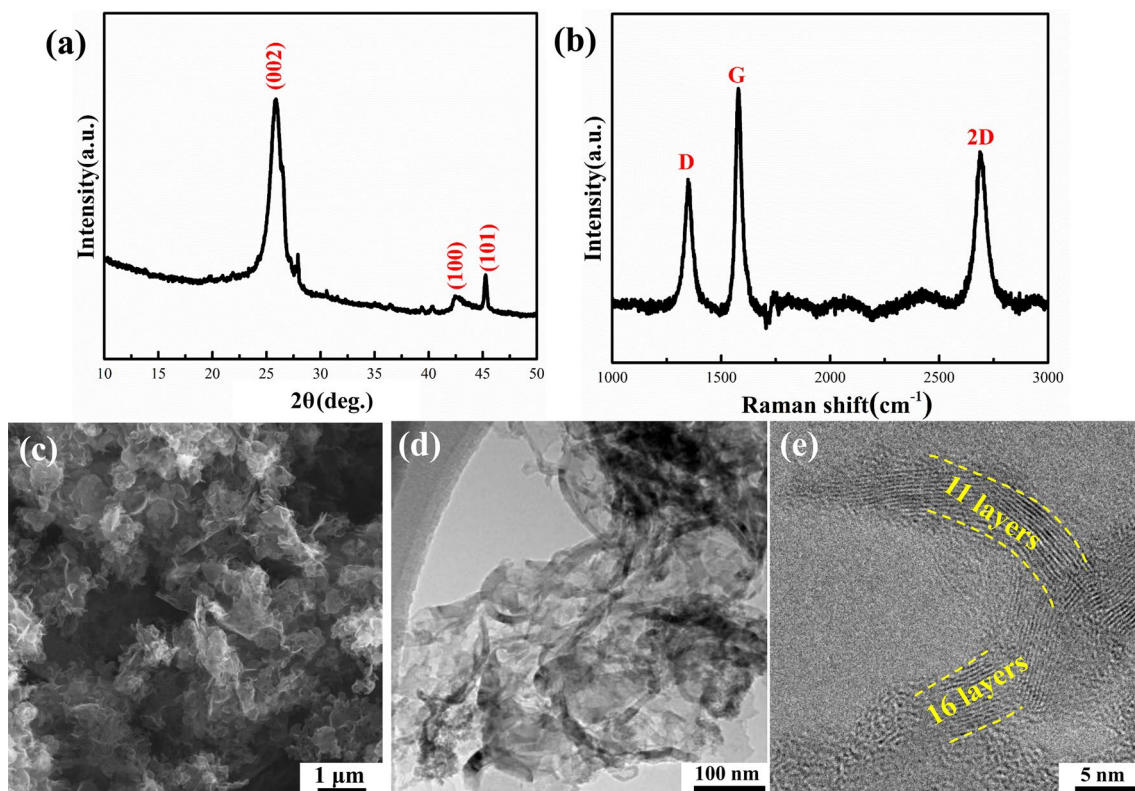


Fig. 2 Characterization of in situ growth of GNPs powder: **a** XRD result; **b** Raman spectra; **c** SEM observation; **d** TEM observation; **e** high resolution TEM

adapted to clearly reveal the uniform 2D layered morphology with abundant ripples and wrinkle as shown in Fig. 2c, d. High-resolution TEM (HRTEM) image indicates that the GNPs layers could be found at the edges and wrinkles in Fig. 2e. The above results confirm that GNPs can be formed in the molten Mg via in situ process.

3.2 Microstructure of the Composites

Figure 3 displays the XRD patterns of as-cast the Mg6Zn matrix and the GNPs/Mg6Zn composites. The XRD results show the characteristic diffraction peaks of α -Mg phase in the Mg6Zn alloy and the composites. The diffraction peaks of the Mg_4Zn_7 phase in Mg6Zn alloy can also be found in the illustration, but the characteristic peak disappears in the composites. The specific reasons will be considered later. In addition, the content of GNPs in Mg alloy is so low that no obvious diffraction peak corresponding to GNPs was found in the as-fabricated composites. However, 1 mol of GNPs would form 2 mol of MgO simultaneously by Eq. 1. Thus, it could be calculated that the content of MgO is significantly higher than that of GNPs in the composites. As a result, the peaks corresponding to MgO phase could be observed in the 0.28GNPs/Mg6Zn composites.

Figure 4a–c shows SEM observation of Mg6Zn alloy and the GNPs/Mg6Zn composites after solidification. The microstructure of the Mg6Zn alloy can be determined including primary α -Mg and eutectic structure (α -Mg + β - Mg_4Zn_7) as shown in Fig. 4a, and the eutectic structure is indicated by the blue arrow. In comparison, apart from to the morphology of the primary α -Mg and eutectic structure, a new phase morphology can also be observed by the yellow arrow in Fig. 4b, c. EDS analysis was used to analyze the composition

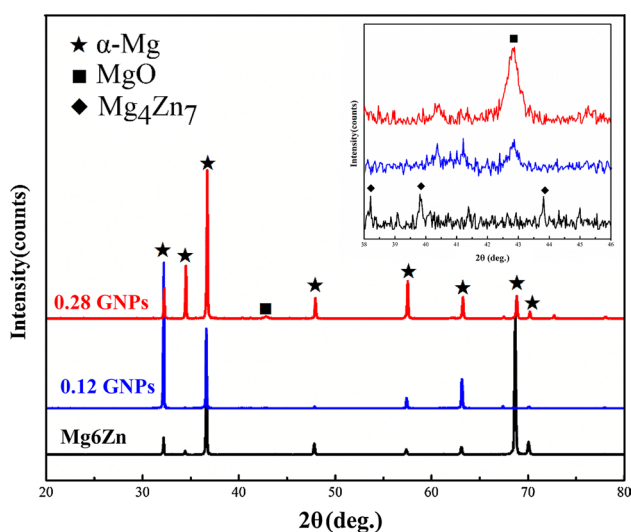


Fig. 3 XRD patterns of Mg6Zn alloy, GNPs/Mg6Zn composites

of these dispersed phases. As shown in Fig. 5, the distribution of C, O, Mg and Zn element in the composite can be clearly found. The positions of C, O and Zn in EDS spectra correspond to in situ grown GNPs, MgO and the eutectic phase of Mg_4Zn_7 , respectively. As shown in Fig. 5, it clearly shows that these dispersed phases were identified as the in situ grown GNPs through obvious carbon enrichment. Besides, the distribution of O element comes from the high coincidence of MgO and C elements, indicating that the MgO is distributed on GNPs surface. Thus, the SEM micrographs show that the MgO modified GNPs were incorporated and dispersed into the Mg matrix well.

Furthermore, compared with Mg6Zn alloy, it can be found that the morphology and size of the eutectic structure are also changed in the composites as shown in Fig. 4d. The increase in GNPs content in Mg matrix causes the remarkable morphological transformation of eutectic structure from flaky to sphericity. At higher magnification, it can even be found that GNPs are distributed in eutectic phase individually as illustrated in Fig. 4d, which also leads to the refinement of coarse eutectic structure in the composites. For the Mg6Zn alloy, the content of Zn element is less than the eutectic point, thus the α -Mg is precipitated first during solidification. With the precipitation of α -Mg, the excess Zn element will be continuously discharged to the liquid region, resulting in the increase in Zn content in the liquid region. When the composition in the liquid region reaches the eutectic point, the eutectic reaction will be formed. In the GNPs/Mg6Zn composites, in situ GNPs with large specific surface area can inhibit the discharge of Zn from the first formed α -Mg. Thus, high content of Zn can be dissolved in α -Mg. This also makes it difficult for the composition of the liquid region to reach the eutectic point. Finally, the size and content of eutectic phase in the composites have changed evidently. Consequently, the diffraction peak of the second phase was not observed in the composites in the XRD patterns.

Figure 6 shows the SEM images of the Mg6Zn alloy and composites by hot extrusion. It could be found that the GNPs in the as-cast composite are broken to a certain extent, resulting in a uniform band-like distribution parallel to the extruded direction. In addition, the OM images reveal that all the samples are dynamically recrystallized grain. The average grain size in Mg6Zn alloy, 0.12 GNPs/Mg6Zn and 0.28 GNPs/Mg6Zn composites is 10.4 μ m, 4.5 μ m and 3.0 μ m, respectively. In order to coordinate deformation, high density geometric dislocations can be generated around GNPs, which can stimulate more nucleation of dynamic recrystallization. Meanwhile, the grain boundary pinning effect of GNP also effectively restricts the growth of recrystallized grains [27–29]. Thus, the grain size of the as-extruded composites is much lower than Mg alloys under the same processing conditions.

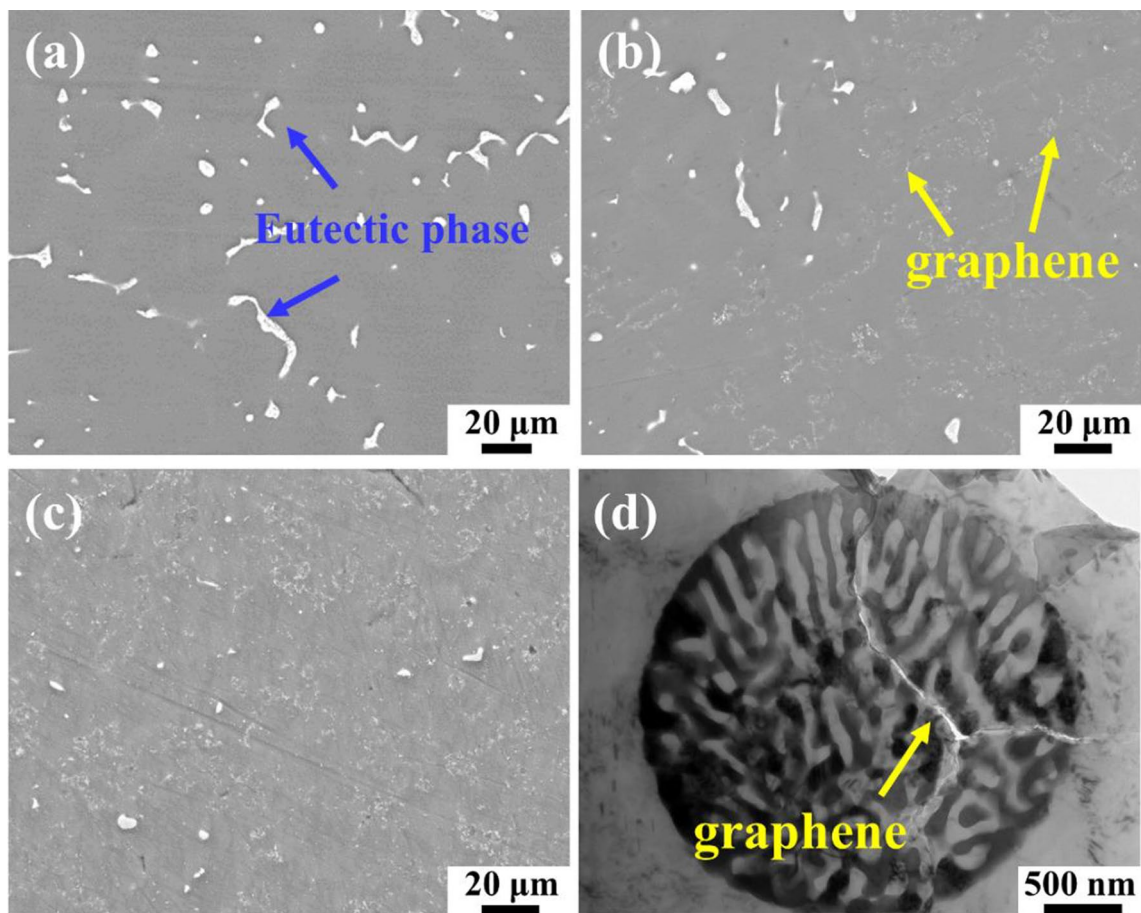


Fig.4 Microstructures of as-cast samples after solidification: **a** Mg6Zn alloy matrix; **b** 0.12 GNPs/Mg6Zn composites; **c** 0.28 GNPs/Mg6Zn composites. **d** Eutectic structure in composites

Figure 7(a) reveals the morphology of MgO modified GNPs in Mg matrix composites, no voids were observed at the interface, indicating the formation of a tight interface structure. Figure 7b shows the interfacial structure of the composite between GNPs and Mg matrix. GNPs can be clearly distinguished by measuring the layer spacing of (002) crystal surface (0.34). It also demonstrates that the MgO particles are located at the interfacial position between Mg matrix and GNPs. Previous reports have proved that the C atoms of GNPs could be connected with the surface of MgO nanoparticles tightly. The reason is that a nanoscale-contact and diffused bonding interface were achieved between MgO and GNPs in the composites [30, 31]. Based on the above results, the MgO nanoparticles in interfacial area performed like “stitches”, could enhance the interfacial strength of the Mg matrix composites.

The above results show that the in situ liquid-state method realizes the interface modification between GNPs and Mg matrix. For metal matrix composites, the interface is an important medium to connect the reinforcement

with the metal matrix. Most of the macroscopic mechanical properties of composites depend on the interfacial structure. For the unique two-dimensional morphology and high specific surface area of GNPs, it can form more interface contact with the matrix, which makes the interface between the metal matrix and GNPs more important than the traditional reinforcement. However, Mg cannot be wetted with GNPs even above the melting point due to the different chemical properties. GNPs are usually in the state of directly embedded in the metal matrix, no chemical connection was formed between them. Thus, weak interfacial strength is a typical problem that limits the development of composites. Traditional interface modification usually adopts surface modification of graphene, micro-alloying and graphene defect engineering [32, 33]. Complex process hinders the further development of metal matrix composites. In comparison, the in situ reactive process provides a simple and feasible idea to improve the interfacial strength.

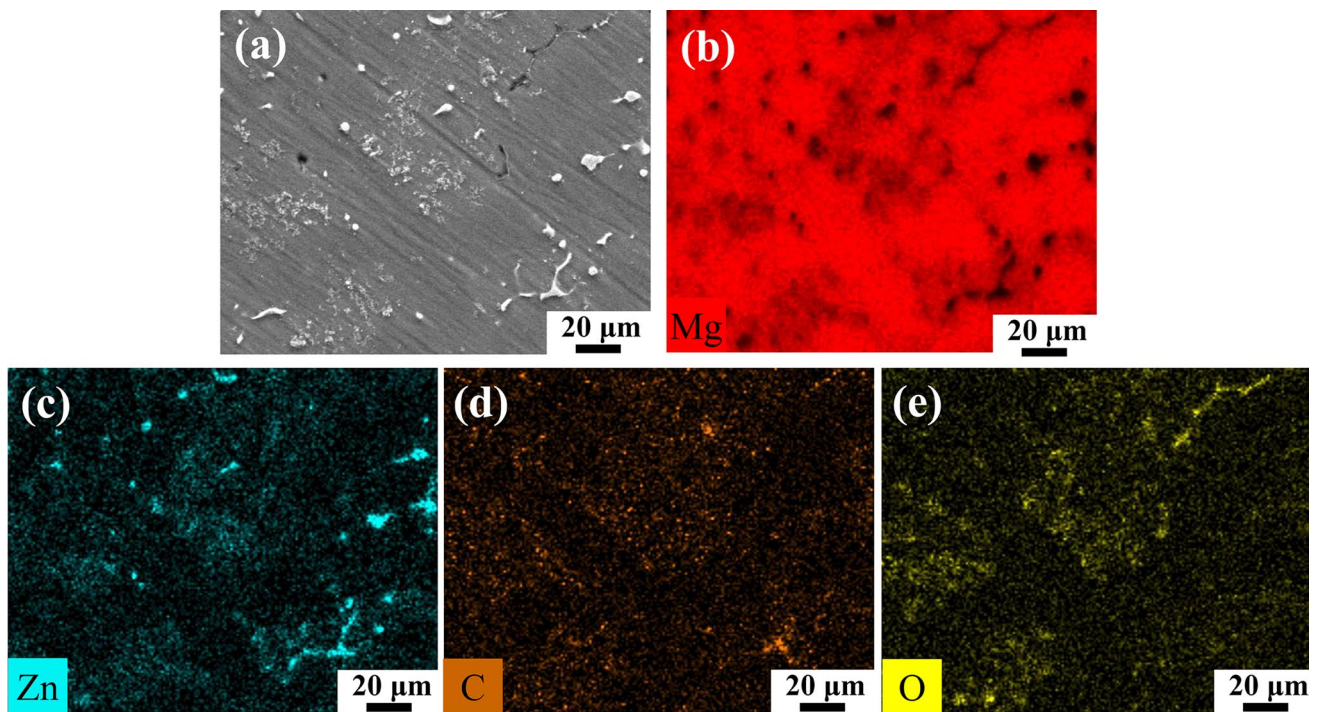


Fig. 5 a SEM image; b–e element distributions of Mg, Zn, C, O

3.3 Mechanical Properties

Tensile stress–strain curves of the Mg6Zn alloy and GNPs/Mg6Zn composites are shown in Fig. 8. With increasing GNPs content, the tensile strength of the composites is enhanced significantly compared with that of the unreinforced Mg alloys. The yield strength (YS) of Mg6Zn alloy is 168 MPa. 0.12 GNPs/Mg6Zn and 0.28 GNPs/Mg6Zn composites own higher YS, reaching the 195 MPa and 206 MPa, respectively. It is indicated that composites have a significant improvement in the strength by in situ grown GNPs. In our experiment, the obtained composites exhibit uniform dispersion of GNPs, strong interfacial bonding between GNPs and matrix, which is essential for achieving high load-transfer efficiency. Therefore, the load-transfer strengthening from Mg matrix to GNPs increases part of the yield strength of composites. On the one hand, it can be seen that the addition of GNPs leads to an obvious grain refinement in Fig. 6, the fine grain hinders the movement of dislocations and results in an accumulation of dislocations on the grain boundaries. The contribution of grain refinement can be reflected in the Hall–Petch relation [34–37]. Besides, the accumulation of dislocations at the interface is also helpful to increase the strength of the composite due to the large difference between the thermal expansion coefficients of GNP and Mg matrix [38, 39]. Therefore, the as-fabricated composites show higher YS compared with the Mg6Zn alloy.

In addition, tensile strain of the composite is the highest (27.6%) when the weight fraction of GNPs is 0.12 wt%, and it decreases when the content of GNPs is from 0.12 wt% to 0.28 wt%. This is because small amount of GNPs can suppress localized deformation along basal slip planes and enabling the activation of other potential slip systems [34]. When the GNPs content further increases, the composites may generate strong strain localization because the plastic deformation of the matrix is hindered. Thus, the strain localization around the GNP finally leads to the matrix cracking between the matrix and GNP [40]. Finally, the elongation of 0.28GNPs/Mg6Zn composites decreases to a certain extent (15.6%).

4 Conclusion

The GNPs/Mg6Zn composites were fabricated using in situ liquid-state method. The distribution of GNPs is uniform while the morphology and size of the eutectic phase are also changed in the as-cast composites. The grain size of the matrix in the GNPs/Mg6Zn composites decreases with increasing content of the GNPs compared with the Mg6Zn alloy. Tensile strength of the GNPs/Mg6Zn composites is increased with increasing content of the GNPs. Meantime, the composites also exhibit a notable plastic deformation stage, and especially the ductility of 0.12 GNPs/Mg6Zn composites reaches 27.6%. Therefore, this novel preparation

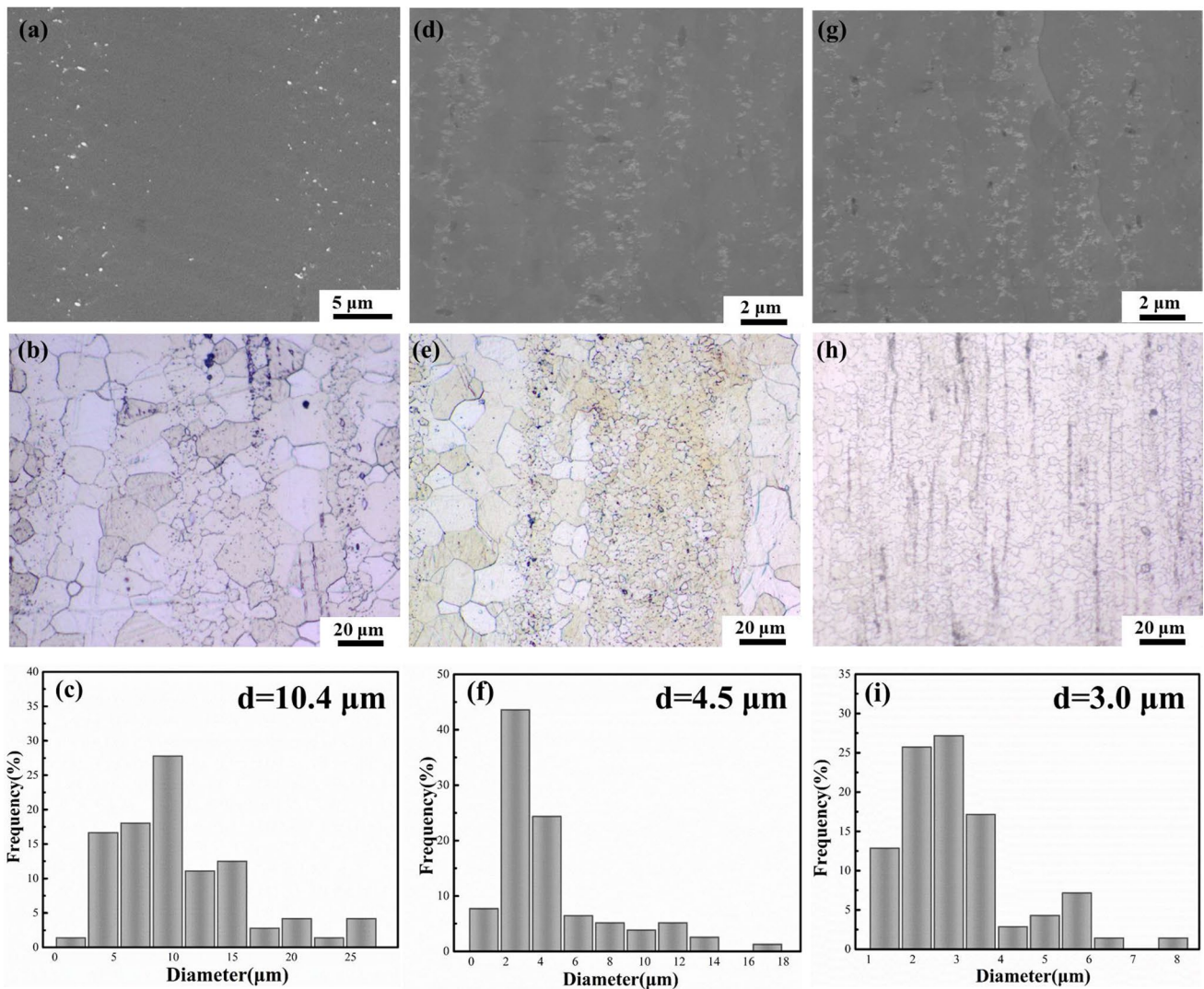


Fig. 6 SEM images, OM images and grain size distributions: **a–c** Mg6Zn alloy; **d–f** 0.12GNPs/Mg6Zn composites; **g–i** 0.28GNPs/Mg6Zn composites

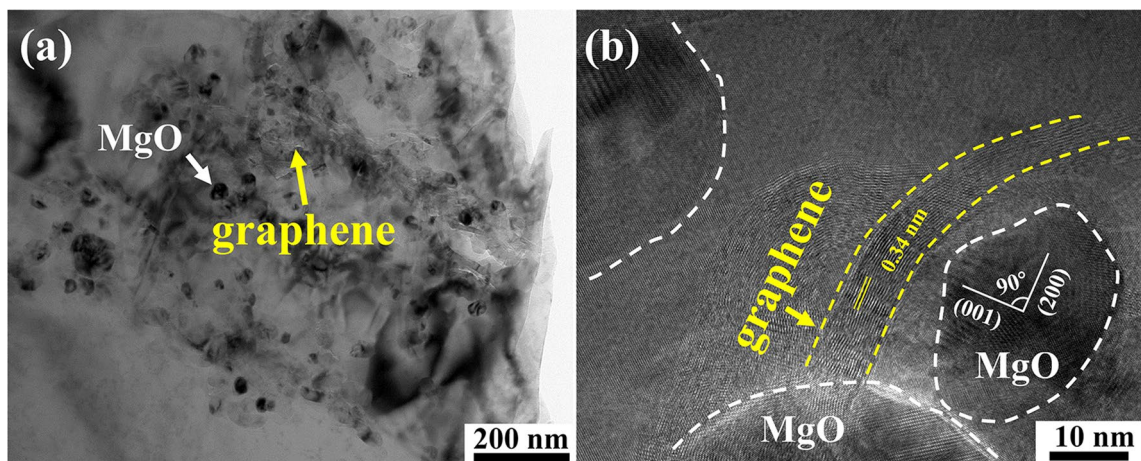


Fig. 7 **a** TEM image of the composite; **b** interface between GNPs, Mg matrix

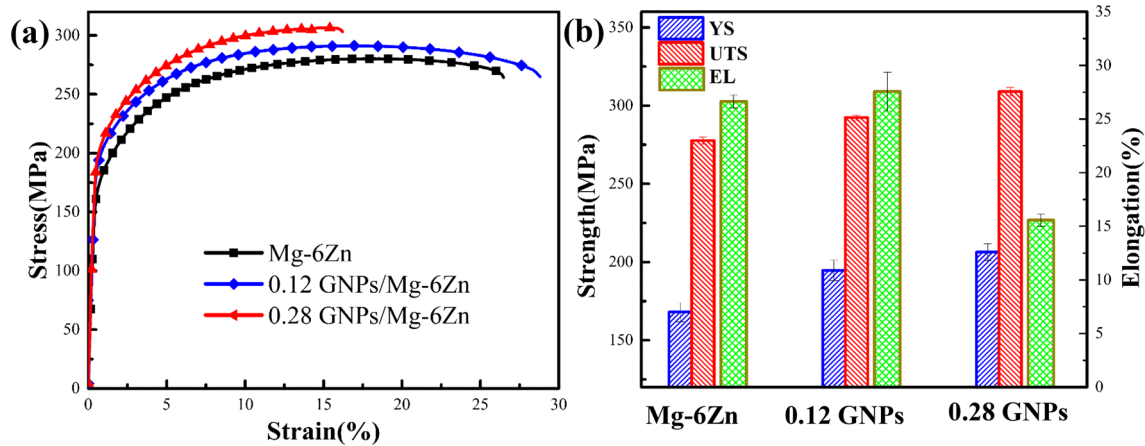


Fig. 8 **a** Tensile stress–strain curves of the as-extruded samples; **b** comparison between the different materials

method has great application potential in preparing high strength and high ductility Mg matrix composites.

Acknowledgements This work was supported by the National Natural Science Foundation of China (Grant Nos. 51871074, 51971078).

Declarations

Conflict of interest The authors state that there are no conflicts of interest to disclose.

References

- [1] K.B. Nie, X.J. Wang, K.K. Deng, X.S. Hu, K. Wu, J. Magnes. Alloys. **9**, 57 (2021)
- [2] S. Ataya, N.A. Alsaleh, E.S. Seleman, Acta Metall. Sin. -Engl. Lett. **32**, 31 (2019)
- [3] B. Tang, J.B. Li, J.L. Ye, H. Luo, Y.T. Wang, B. Guan, Y.F. Lu, X.H. Chen, K.H. Zhen, F.S. Pan, Acta Metall. Sin. -Engl. Lett. **35**, 1935 (2022)
- [4] X. Cai, S.J. Ding, Z.J. Li, X. Zhang, K.K. Wen, L.D. Xu, Y. Zhang, T.D. Shen, Compos. Pt. B-Eng. **215**, 108743 (2021)
- [5] P. Xiao, Y.M. Gao, C.C. Yang, Y.F. Li, X.Y. Huang, Q.K. Liu, S.Y. Zhao, F.X. Xu, M. Gupta, Compos. Pt. B-Eng. **198**, 108174 (2020)
- [6] W.J. Li, K.K. Deng, X. Zhang, C.J. Wang, J.W. Kang, K.B. Nie, W. Liang, J. Alloys Compd. **695**, 2215 (2016)
- [7] K.S. Novoselov, A.K. Geim, S.V. Morozov, D. Jiang, Y. Zhang, S.V. Dubonos, I.V. Grigorieva, A.A. Firsov, Science **5**, 1 (2004)
- [8] A.C. Ferrari, D.M. Basko, Nat. Nanotechnol. **8**, 235 (2013)
- [9] W. Kong, H. Kum, S.H. Bae, J. Shim, H. Kim, L. Kong, Y. Meng, K. Wang, C. Kim, J. Kim, Nat. Nanotechnol. **14**, 927 (2019)
- [10] K.R. Nandanapalli, D. Mudusu, S. Lee, Carbon **15**, 2954 (2019)
- [11] L.D. Wang, Z.Y. Yang, Y. Cui, B. Wei, S.C. Xu, J. Sheng, M. Wang, Y.P. Zhu, W.D. Fei, Sci. Rep. **7**, 41896 (2017)
- [12] J.C. Li, X.X. Zhang, L. Geng, Compos. Pt. A- Appl. Sci. Manuf. **121**, 487 (2019)
- [13] D. Li, C. Wang, Y.S. Su, D. Zhang, Q.B. Ouyang, Acta Metall. Sin. -Engl. Lett. **33**, 649 (2020)
- [14] F. Chen, J. Ying, Y. Wang, S. Du, Z. Liu, Q. Huang, Carbon **96**, 836 (2016)
- [15] G. Liu, N. Zhao, C.S. Shi, E.Z. Liu, F. He, L.Y. Ma, Q.Y. Li, J.J. Li, C.N. He, Mater. Sci. Eng. A **699**, 24 (2017)
- [16] Q.H. Yuan, X.S. Zen, Y. Liu, L. Luo, J.B. Wu, Y.C. Wang, G.H. Zhou, Carbon **96**, 843 (2016)
- [17] Q.H. Yuan, G.H. Zhou, L. Liao, Y. Liu, L. Luo, Carbon **127**, 177 (2018)
- [18] S.L. Xiang, X.J. Wang, M. Gupta, K. Wu, X.S. Hu, M.Y. Zheng, Sci. Rep. **6**, 1 (2016)
- [19] M. Wang, Y. Zhao, L. Wang, Y. Zhu, X.J. Wang, J. Sheng, Z. Yang, H. Shi, Z. Shi, W. Fei, Carbon **963**, 139954 (2018)
- [20] X.J. Li, X.J. Wang, X.S. Hu, C. Xu, W.Z. Shao, K. Wu, J. Magnes. Alloys. In press (2021)
- [21] X.J. Li, H.L. Shi, X.J. Wang, X.S. Hu, C. Xu, W.Z. Shao, Carbon **186**, 632 (2022)
- [22] Q. Miao, L.D. Wang, Z. Liu, B. Wei, F.B. Xu, W.D. Fei, Sci. Rep. **6**, 1 (2016)
- [23] X.J. Li, H.L. Shi, X.J. Wang, X.S. Hu, C. Xu, W.Z. Shao, J. Alloys Compd. **921**, 165938 (2022)
- [24] S.H. Wei, H.L. Shi, X.J. Li, X.J. Wang, X.S. Hu, C. Xu, J. Alloys Compd. **902**, 163700 (2022)
- [25] X.J. Li, H.L. Shi, X.J. Wang, X.S. Hu, C. Xu, W.Z. Shao, Compos. Pt. A- Appl. Sci. Manuf. **161**, 107079 (2022)
- [26] Y. Tang, P. Peng, S. Wang, Z. Liu, X. Zu, Q. Yu, Chem. Mater. **29**, 8404 (2017)
- [27] K.K. Deng, X.J. Wang, M.Y. Zheng, K. Wu, Mater. Sci. Eng. A **560**, 824 (2013)
- [28] S. Nam, K. Chang, W. Lee, M.J. Kim, J.Y. Hwang, H. Choi, Sci. Rep. **8**, 1 (2018)
- [29] N. Hansen, B. Bay, J. Mater. Sci. **7**, 1351 (1972)
- [30] Z. Zhao, P. Bai, W. Du, B. Liu, D. Pan, R. Das, C.T. Liu, Z. Guo, Carbon **170**, 302 (2020)
- [31] X. Du, W.B. Du, Z. Wang, K. Liu, S. Li, Appl. Surf. Sci. **484**, 414 (2019)
- [32] X.J. Zhang, Z.K. Dai, X.R. Liu, W.C. Yang, H. Meng, Z.R. Yang, Acta Metall. Sin. -Engl. Lett. **31**, 761 (2018)
- [33] Y.X. Lu, F. Luo, Z. Chen, J. Cao, K. Song, L. Zhao, X.L. Xu, W.Y. Li, Acta Metall. Sin. -Engl. Lett. **1**, 17 (2022)
- [34] Y.Y. Xiang, X.J. Wang, X.S. Hu, L.L. Meng, Z.X. Song, X.J. Li, Z.M. Sun, Q. Zhang, K. Wu, Compos. Pt. A- Appl. Sci. Manuf. **119**, 225 (2019)
- [35] C.D. Li, X.J. Wang, W.Q. Liu, K. Wu, H.L. Shi, C. Ding, X.S. Hu, M.Y. Zheng, Mater. Sci. Eng. A **597**, 264 (2014)
- [36] X. Zhang, C.S. Shi, E.Z. Liu, F. He, L.Y. Ma, Q.Y. Li, J.J. Li, B. Wolfgang, N.Q. Zhao, C.N. He, Nanoscale **9**, 11929 (2017)

- [37] M. Wang, L.D. Wang, J. Sheng, Z.Y. Yang, Z.D. Shi, Y.P. Zhu, J. Li, W.D. Fei, *J. Alloys Compd.* **798**, 403 (2019)
- [38] K.B. Nie, Z.H. Zhu, P. Munroe, K.K. Deng, J.G. Han, *Acta Metall. Sin. -Engl. Lett.* **33**, 122 (2020)
- [39] Z.D. Shi, J. Sheng, Z. Yang, Z. Liu, S. Chen, M. Wang, L.D. Wang, W.D. Fei, *Carbon* **165**, 349 (2020)
- [40] H. Wu, G.H. Fan, *Prog. Mater. Sci.* **113**, 100675 (2020)

Springer Nature or its licensor (e.g. a society or other partner) holds exclusive rights to this article under a publishing agreement with the author(s) or other rightsholder(s); author self-archiving of the accepted manuscript version of this article is solely governed by the terms of such publishing agreement and applicable law.